Structured light generation by magnetic metamaterial half-wave plates at visible wavelength

IOP Publishing Journal of Optics
J. Opt. 19 (2017) 125103 (9pp) https://doi.org/10.1088/2040-8986/aa95dc

Structured light generation by magnetic metamaterial half-wave plates at visible wavelength

Jinwei Zeng[1], Ting S Luk[2], Jie Gao[1,3] and Xiaodong Yang[1,3]

[1] Department of Mechanical and Aerospace Engineering, Missouri University of Science and Technology, Rolla, MO 65409, United States of America
[2] Center for Integrated Nanotechnologies, Sandia National Laboratories, Albuquerque, NM 87185, United States of America

E-mail: gaojie@mst.edu and yangxia@mst.edu

Received 30 June 2017, revised 16 October 2017
Accepted for publication 25 October 2017
Published 17 November 2017

Abstract

Metamaterial or metasurface unit cells functioning as half-wave plates play an essential role for realizing ideal Pancharatnam–Berry phase optical elements capable of tailoring light phase and polarization as desired. Complex light beam manipulation through these metamaterials or metasurfaces unveils new dimensions of light–matter interactions for many advances in diffraction engineering, beam shaping, structuring light, and holography. However, the realization of metamaterial or metasurface half-wave plates in visible spectrum range is still challenging mainly due to its specific requirements of strong phase anisotropy with amplitude isotropy in subwavelength scale. Here, we propose magnetic metamaterial structures which can simultaneously exploit the electric field and magnetic field of light for achieving the nanoscale half-wave plates at visible wavelength. We design and demonstrate the magnetic metamaterial half-wave plates in linear grating patterns with high polarization conversion purity in a deep subwavelength thickness. Then, we characterize the equivalent magnetic metamaterial half-wave plates in cylindrical coordinate as concentric-ring grating patterns, which act like an azimuthal half-wave plate and accordingly exhibit spatially inhomogeneous polarization and phase manipulations including spin-to-orbital angular momentum conversion and vector beam generation. Our results show potentials for realizing on-chip beam converters, compact holograms, and many other metamaterial devices for structured light beam generation, polarization control, and wavefront manipulation.

Keywords: optical vortex beam, vector beam, magnetic metamaterials, half-wave plates, Pancharatnam–Berry phase optical elements

(Some figures may appear in colour only in the online journal)

1. Introduction

The recent discovery and development of structured light including optical vortices and vector beams have driven a revolutionary advance in modern optics and photonics [1, 2]. Structured light is identified by its unique spatially-inhomogeneous distribution of intensity, phase or polarization, showing unprecedented potentials in quantum communication, sensing, imaging, and optical manipulation [3–9]. In general, it is difficult to generate or manipulate structured light using natural existing materials, especially in microscopic scale, due to the lack of strong anisotropy induced significant wavefront modulation. Such limitation has been largely overcome by the merging of structured light with artificially structured media [1, 2], including metamaterials and metasurfaces which are subwavelength composite

[3] Authors to whom any correspondence should be addressed.

materials with engineered electromagnetic properties such as negative refraction, extraordinary anisotropic dispersion, near-zero permittivity, and optical magnetism [10–17]. With carefully designed unit cells and array patterns, metamaterials and metasurfaces can complexly tailor the light intensity, phase and polarization in a desired manner for producing structured light beams and reconstructing holographic images [2, 9, 14–16, 18–31].

One major approach to generate and manipulate structured light is to utilize the space-domain Pancharatnam–Berry phase [32, 33], which describes the relationship between phase shift and polarization change while a light beam normally transmits through an anisotropic optical element [19, 34, 35]. The phase shift of the converted orthogonal polarization component transmitted through the Pancharatnam–Berry phase optical element (PBOE) originates from the geometric phase which varies according to the orientation of the element anisotropy. In contrast to the conventional phase element employing a direct optical path difference, the phase modulation from PBOE is irrelevant to the material dispersion so that broadband operation can be realized. Various types of PBOEs such as nanorods, nano-gratings, split-ring antennas, and V-shaped antennas arranged in certain spatially distributed array patterns have been designed to produce scalar or vector vortices with arbitrary orbital angular momentum [16, 18, 22, 25, 27, 36, 37]. However, most of the existing plasmonics based PBOEs especially working at visible wavelength suffer from low polarization conversion purity, defined as the intensity ratio between the converted polarization component and the total transmitted beam, of less than 10%, so that the generated vortex component from the converted polarization component is overwhelmed by the original polarization component [21, 36–38]. Although the generated optical vortices with certain polarization can be typically separated by applying a polarization filter [36] or creating a diffraction grating [37, 39, 40], it is still difficult to separate the generated vector beams with complex polarization topological structures. Therefore, an essential demand of metamaterial or metasurface PBOEs is to increase the polarization conversion purity as close to unity as possible.

The half-wave plate (HWP) is one ideal PBOE where the birefringent phase retardation is equal to π, so that the spin of photon is completely inversed to achieve unity polarization conversion purity in circular polarization (CP) basis [36]. However, it is generally challenging to realize metamaterial or metasurface HWPs in visible spectrum range, mainly due to the specific requirements of both strong phase anisotropy and amplitude isotropy in subwavelength scale [41]. Here, we propose magnetic metamaterial HWPs based on metal-dielectric-metal three-layer structures which can simultaneously exploit the electric field and magnetic field of light at visible wavelength, to fit with the required phase and amplitude manipulation at the same time. We design and demonstrate these magnetic metamaterial HWPs in linear grating patterns for producing half-wave phase retardation and equal transmitted intensity between two orthogonal linear polarization (LP) components around the wavelength of 633 nm, with high polarization conversion purity of 80%. Moreover, the magnetic metamaterial HWPs in concentric-ring grating patterns are designed as unique spin-to-orbital angular momentum beam converters for the generation of structured light beams including both optical vortices and vector beams. Our results can open new degrees of freedom for building on-chip metamaterial beam converters and holograms to manipulate light wavefront and polarization.

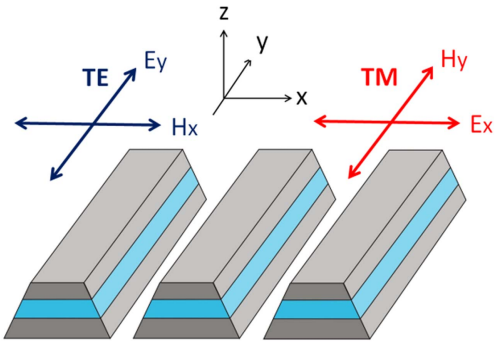

Figure 1. The schematic of metal-dielectric-metal magnetic metamaterial structures and the illustration of TE and TM polarizations.

2. Magnetic metamaterials as HWP in linear grating patterns

A typical magnetic metamaterial structure consists of two parallel metal stripes separated by a dielectric spacer, which is arranged in a subwavelength periodic array pattern as shown in figure 1. Many literatures have interpreted the physical mechanism of this structure to simultaneously exploit the electric field and magnetic field of light [12–14, 16]. Under transverse magnetic (TM) polarization where the incident magnetic field is parallel with the metal stripes, a circulating current loop surrounding the center dielectric spacer is excited by the magnetic field of incident beam to induce a magnetic resonance, exhibiting a transmission minimum with an abrupt phase variation near the resonance wavelength. In the off resonance region under TM polarization, the structure exhibits a smooth variation of transmission phase. Under transverse electric (TE) polarization where the electric field is parallel with the metal stripes, the grating effect makes such structure as a diluted metal with flat transmission profile and continuous phase variation.

Some previous works exploit the strong anisotropic amplitude extinction on the magnetic resonance to make effective linear or vector polarizer [14, 16]. Here we go one step forward to make an effective phase plate by making simultaneous phase anisotropy and amplitude isotropy. A desired phase shift such as half wave retardation at the specified wavelength can be realized by varying the geometry of the structure. But, on the other hand the transmission amplitude proximity between TE and TM polarizations is also challenging. It is difficult to realize for a single-layer metal grating, where the optical resonance will induce not only the phase anisotropy but also the amplitude anisotropy. Here, the magnetic metamaterial structure exhibits unique independent

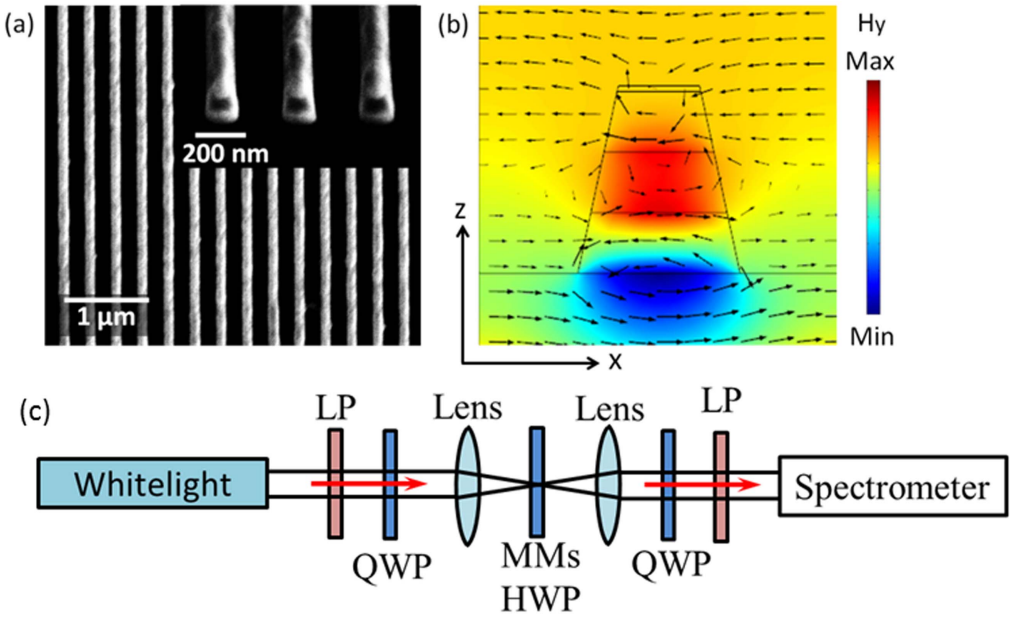

Figure 2. (a) The top view and cross-section SEM images of the fabricated magnetic metamaterial structures in linear grating patterns. (b) The simulated magnetic field (color map) and electric displacement (arrow) distributions at the magnetic resonance in TM polarization. (c) The schematic of optical setup for transmission analysis in circular polarization basis.

magnetic resonance, which is under the orthogonal polarization to the electric grating effect, so that the transmission amplitude equality can be achieved near the magnetic resonance wavelength by both effects. In such a way, the functionality of HWP is realized by a 1D grating pattern in the multilayer, which gives great simplicity and convenience for the design and fabrication processes.

It is noted that the magnetic resonance wavelength is mainly determined by the width of metal stripes and the thickness of dielectric spacer, which is independent on the grating period; while the grating period will affect the grating filling fraction and control the transmitted intensity. By carefully designing the magnetic metamaterial structural parameters including the thickness of metal and dielectric layers, the width of metal stripes and the grating period, both the desired π phase retardation and equal transmitted intensity between TE and TM polarizations can be realized for achieving ideal HWPs in subwavelength scale. This almost 'mutually independent' control over the magnetic resonance and grating effect provides excellent freedom and convenience to design the magnetic metamaterials as wave plates or other purposes, or even tunable optical devices. The possibility and principle of tunable magnetic metamaterial waveplates will be further discussed in a later section.

The magnetic metamaterial structures in linear grating patterns acting as homogeneous HWPs near the wavelength of 633 nm are first designed and tested. The Ag–SiO_2–Ag three-layer structure is deposited on the glass slide by the sputtering method at the deposition rates of 0.4 Å sec^{-1} and 0.2 Å sec^{-1} for Ag and SiO_2 layers, respectively. The thickness of each layer is 55 nm and there is an additional 5 nm thick SiO_2 surface protection layer on top. The optimized structural parameters of the grating period of 300 nm and the bottom width of 140 nm are used by considering the side wall angle of the trapezoidal shape of the structure around 78°. The linear grating patterns are then fabricated by the focus ion beam milling and figure 2(a) shows the SEM image of the sample. Figure 2(b) plots the magnetic field and polarization distributions in TM polarization at the magnetic resonance wavelength of 580 nm simulated by the finite element method (COMSOL), where the measured permittivities of Ag and SiO_2 and the layer thicknesses from the variable angle spectroscopic ellipsometry are employed in simulation. According to the previous numerical studies of the similar structure [12, 13], we slightly adjust the loss of silver, indicated by the imaginary part of silver permittivity, as a reflection of fabrication imperfection to fit the simulated transmission spectrum to experiment for a more accurate phase estimation. An antiparallel current between the two metal strips and the sandwiched magnetic dipole clearly indicate the excitation of magnetic resonance.

The fabricated sample is then characterized by transmission spectroscopy in the visible range with an optical setup including a Halogen white light source and a spectrometer. Figures 3(a) and (c) plot the measured transmission spectra through the linear grating patterns under both LP basis and CP basis, showing good agreement with the simulation results. The simulated transmission phase shifts in TE and TM polarizations are also plotted in figure 3(b). It is shown that near 633 nm the transmitted intensities of TE and TM polarizations are equal to each other and the transmission phase retardation between TE and TM polarizations is around 160° (0.9π), indicating the near-ideal HWP functionalities. For the transmission spectrum characterization under CP basis shown in figure 3(c), the incident beam is set to have right-handed CP (original spin, OS) and the converted spin component in transmission has left-handed CP (converted spin, CS). The converted spin transmission and original spin

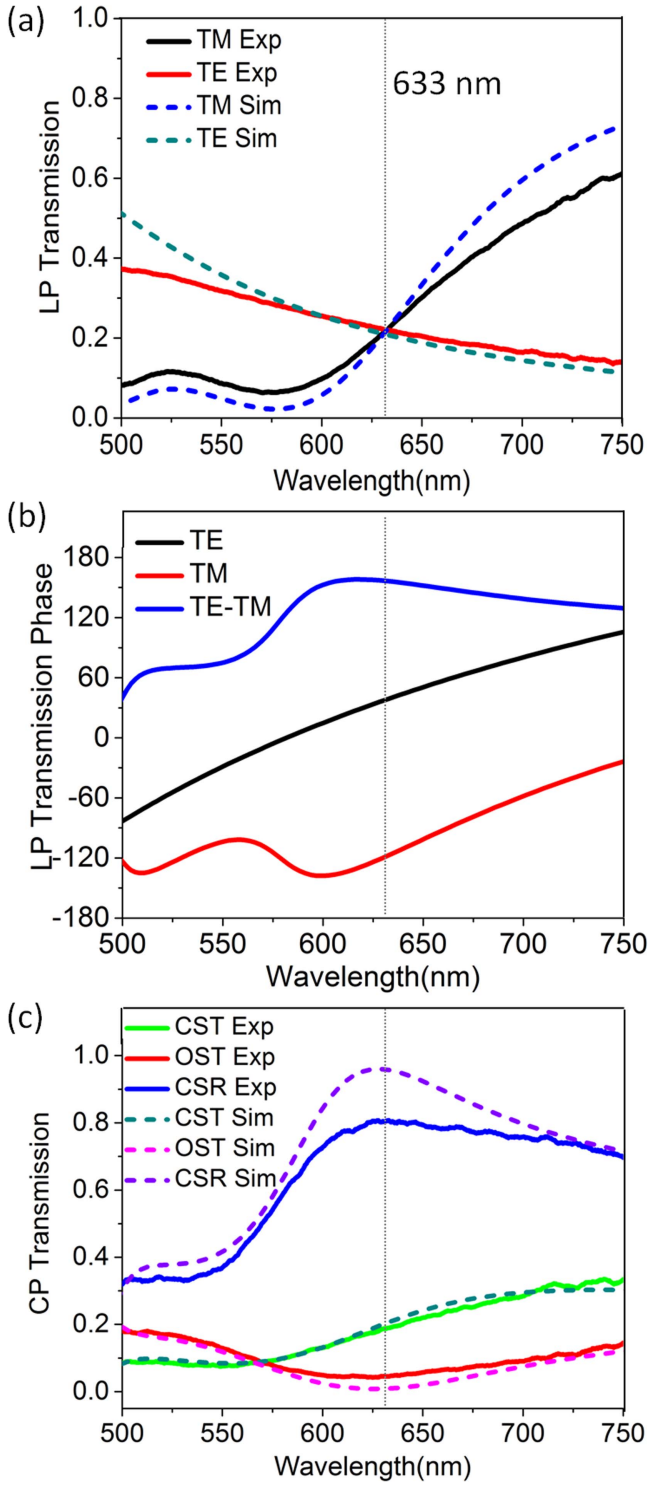

Figure 3. (a) The measured and simulated transmission spectra through the linear grating patterns under linear polarization basis. (b) The simulated transmission phase shifts under linear polarization basis. (c) The measured and simulated converted spin transmission (CST) spectra and original spin transmission (OST) spectra under circular polarization basis, as well as converted spin ratio (CSR).

transmission (OST) are defined as the intensity in OS or CS component in the transmitted beam divided by the incident beam intensity, respectively. The polarization conversion purity, which can be defined as the converted spin ratio (CSR) —the intensity of the converted spin component divided by the total intensity of the transmitted beam, is also plotted. The measured polarization conversion purity is around 80% at 633 nm, proving that our designed magnetic metamaterial structures work well as decent HWPs. It is noteworthy that the experimental OST near the designated HWP wavelength at 633 nm is slightly larger than the simulated OST, thus causing a smaller experimental CSR than the simulated CSR. This is because in CP analysis we have used the set of QWP and LP, in which the QWP (Thorlabs AQWP05M-600) is imperfect that does not have exact 90° phase retardation. The imperfect QWP induces an incomplete circular to LP conversion. As a result, in OST measurement the CP analyzer which is supposed to completely filter out OS component instead allows a small portion of such component to leak through, and therefore falsely suggest a higher OST and a lower CSR in the analyzed beam in experiment.

It is also observed from figure 3(a) that the transmission under LP from the magnetic metamaterial structure is relatively low at around 25%. In order to achieve an excellent HWP PBOE element, it is critically important to realize high polarization conversion purity, which represents the purity of the converted spin in the total transmitted beam with effective phase modulation under PBOE principle. According to figure 3(b), the simulated phase retardation between TE and TM polarizations for the current design is around 160°, less than 180°. In principle, the conversion purity can still be increased by further increasing the thickness of multilayer structure to enhance the phase anisotropy. However, due to the loss of metal which weakens the magnetic resonance that produces the abrupt phase change, further increasing the metal thickness will slowly increase the phase anisotropy but rapidly decrease the overall intensity transmission. Eventually, the current design shown here is optimized to balance between the polarization conversion purity and the transmitted intensity.

Comparing the performance of our transmission-type magnetic metamaterial HWP and other published works, it is reported that both the reflection-type plasmonic metasurface elements and the transmission-type dielectric optical elements [25, 27, 29, 41–45], can simultaneously achieve near-unity polarization conversion purity and energy efficiency. First, as a comparison to reflection-type plasmonic PBOEs, the transmission-type optical elements are often desirable in many circumstances since the latter generally suffers much less beam-steering error from imperfect normal incidence. Comparing to the reported transmission-type dielectric PBOEs, our structure has lower polarization conversion purity and much lower transmission; but on the other hand, it boasts some unique merits in other aspects. Most importantly, the magnetic metamaterials contain multilayered longitudinal cavity that supports magnetic resonance stronger than most resonances induced by single layer structures. *The stronger resonance facilitates our structure to realize desired phase retardation in a thinner thickness (as about a quarter of one wavelength).* As a comparison, the reported dielectric optical elements require the thickness usually close to one wavelength to achieve the desired phase retardation. The

subwavelength thickness of our structure not only boasts a relatively easier fabrication for a smaller height-to-width aspect ratio, but much more importantly it enables the physical approximation of our structure as an optical 'surface' [21]. Phase element can be perfect only from an optical surface, i.e. metasurfaces, which has minimum angular dispersion with better tolerance in small oblique incidence [21, 22]. While, the optical 'bulky' materials that contain wavelength comparable or thicker thickness suffers much greater error in the same oblique illumination.

Another interesting topic is the potential tunability of the magnetic metamaterials with multi-functionalities. Particular PBOE structures can be designed to act as switchable optical components, for example linear polarizers, vector beam converters, and wave plates, by varying operation wavelength, temperature, structure dimension, and other physical parameters [46, 47]. As introduced previously, the magnetic metamaterials studied here exhibit orthogonal-polarization manipulation on light by both magnetic resonance and electric grating effect which are significantly different. Then it is possible to accordingly design the TE and TM spectra of the structure to contain several wavelength locations where it shows different functionalities. For example, the previous works demonstrate that the magnetic metamaterials can be designed as switchable linear polarizers or vector beam converters [14, 16] by tuning the structure either on or off magnetic resonance in different operation wavelengths or structure dimensions. The similar principle can also be applied to wave plates, by designing the spectra of the structure under orthogonal polarizations to contain two or more amplitude-coincident wavelengths with different phase shifts.

3. Magnetic metamaterials as HWP in concentric-ring grating patterns

Next, the magnetic metamaterial structures in concentric-ring grating patterns are fabricated and characterized, where these patterns are equivalent to the transformation of linear grating patterns from Cartesian coordinate to cylindrical coordinate, i.e. the pitch period between the center points in two adjacent rings is 300 nm and the bottom width of each ring is 140 nm on the Ag–SiO_2–Ag multilayer with each layer 55 nm thick. We assume such structure will function as the azimuthally rotated HWPs, and this assumption will be verified by studying both the phase and polarization manipulability from this structure.

Starting from phase manipulation, under circular polarized beam incidence, such structure is expected to act as a spin-to-orbital converter. When a circularly polarized incident beam normally transmits through the sample, the output beam will contain the converted spin component with the opposite CP. According to the PBOE principle, the transmission phase shift difference of the converted spin component between two tilted optical elements equals to twice of their orientation angle [19]. In our concentric-ring grating patterns, a full 2π rotation angle of the magnetic metamaterial HWPs along the azimuthal circle is used so that the phase shift difference of the converted spin component around the center will be 4π. Therefore, an optical vortex beam with topological charge of $+2$ or -2 is expected in the converted spin component for right-handed or left-handed circularly polarized incident beam, respectively. Figure 4(a) shows the fabricated magnetic metamaterial structures in concentric-ring grating patterns. The sample is divided into four sections during the fabrication so that the section boundaries due to slight stitching mismatch are shown in the SEM image. The consequence of the stitching error will be discussed later in this paper. The interferometry experiment is performed to characterize the generated optical vortex from the sample. The input circularly polarized beam from a HeNe laser at 633 nm is focused through the sample by an objective lens at normal incidence. The converted spin component in the transmitted beam is then interfered with the spherical reference beam under the same polarization to form an interference pattern captured by a CCD camera. Figures 4(b) and (c) display the intensity profile of the generated optical vortex and the corresponding interferometry pattern under incident right-handed CP. The intensity profile gives a donut shape around the phase singularity at the beam center. The interferometry image exhibits a double-spiral pattern following counter-clockwise helical orientation, showing the creation of an optical vortex with topological charge of $+2$ (which shows some trend of splitting, and we will explain this in the next section). Figures 5(a) and (b) display the numerically simulated intensity distribution and phase profile of the converted optical vortex transmitted through the 3D concentric-ring grating patterns (containing 7 rings) under incident right-handed CP. The phase variation from 0 to 4π indicates that the optical vortex with orbital angular momentum of $+2$ is generated, which agrees with our theory and experiment.

Furthermore, we study the polarization manipulation of the concentric-ring grating patterned magnetic metamaterial structure by transmitting it with a vertically linear polarized beam. In general HWP is capable to rotate the polarization of the incident linear polarized beam for an angle twice as the angle between the incident LP direction and the fast-axis orientation of the HWP, while maintaining its phase. Therefore, for the circumstance of vertically linear polarized beam transmitting the assumed azimuthal HWPs, the output beam is expected to have a spatially inhomogeneous LP profile, in which the rotated polarization angle will be 4π along the azimuthal circle, i.e. a vector beam, with polarization topological charge 2. Figure 5(c) displays the simulated intensity and polarization distributions of the produced vector beam under incident vertical LP, giving the spatially inhomogeneous LP distribution as expected. Figures 6 and 7 show the measured transmitted images of output vector beams under incident vertical and horizontal LPs, respectively, by placing a rotating LP analyzer before the CCD camera. The beam transmission patterns always exhibit four bright outer lobes rotating together with the analyzer, where the rotation speed of the lobes is half as the rotation speed of the linear analyzer. For instance, as shown in figure 6 while the linear analyzer rotates from 0° to 90°, the bright lobes rotate from $+/-45°$

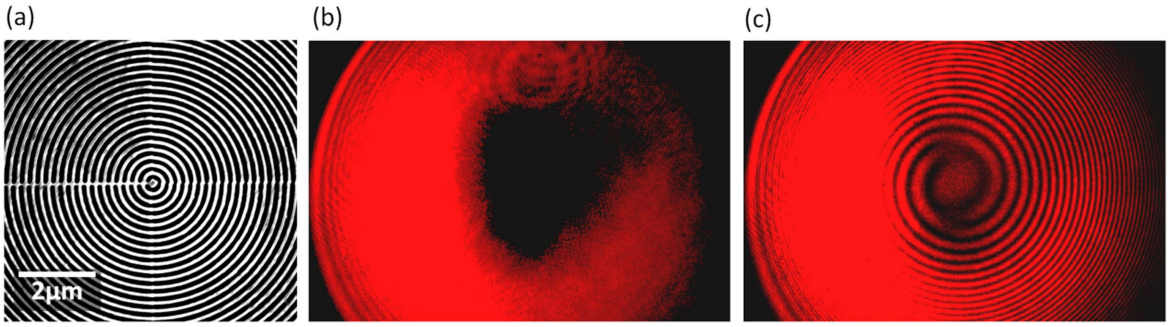

Figure 4. (a) The top view SEM image of the fabricated magnetic metamaterial structures in concentric-ring grating patterns. (b), (c) The captured images of the intensity profile and interferometry pattern of the generated optical vortex at 633 nm, respectively.

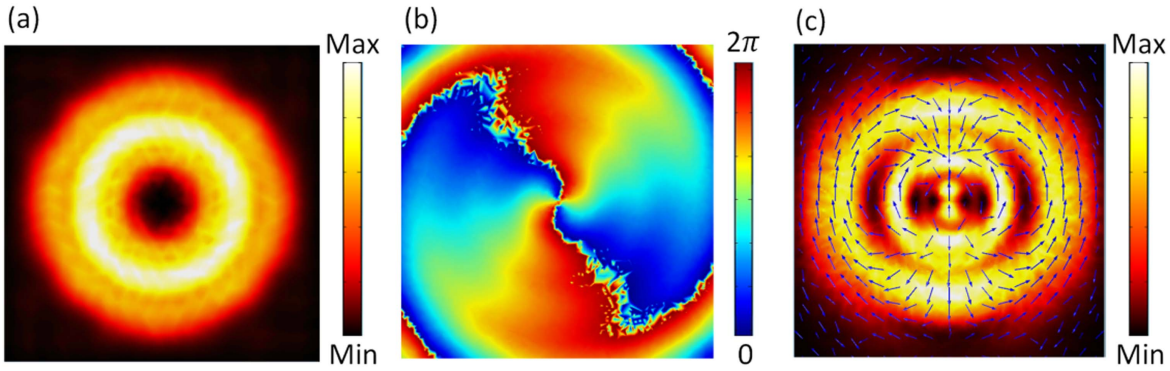

Figure 5. (a), (b) The simulated near-field intensity distribution and phase profile of the generated optical vortex in the transmitted beam under incident right-handed circular polarization. (c) The simulated near-field intensity (color map) and polarization (arrow) distributions of the transmitted vortex beam under incident vertical linear polarization.

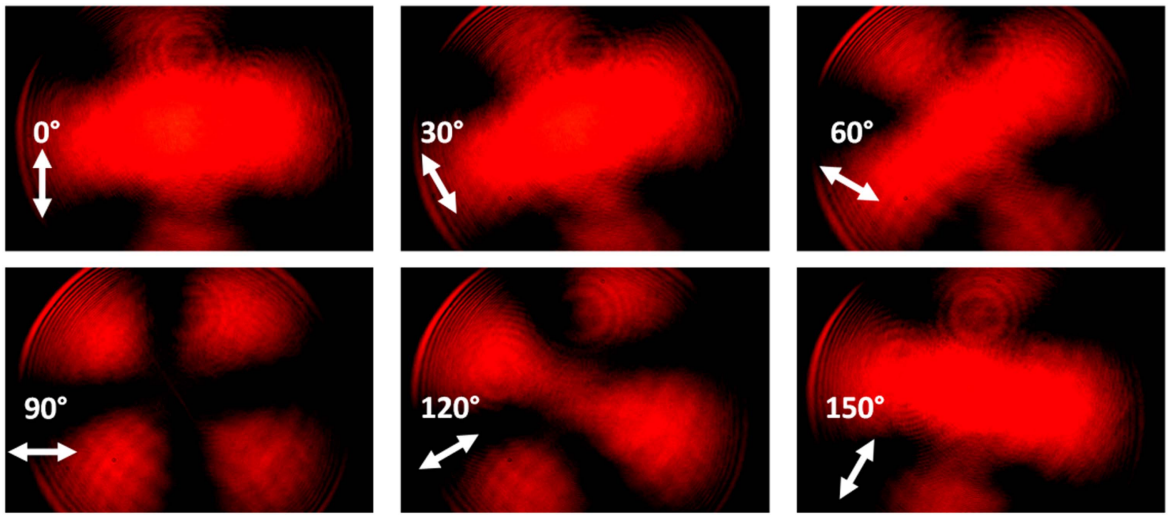

Figure 6. The measured beam transmission images after passing through a rotating polarization analyzer under incident vertical linear polarization. The white arrows represent the analyzer orientation angle from 0° to 150° with a rotation step of 30°.

directions to vertical and horizontal directions, respectively. The lobe-patterns between the incident vertically and horizontally LP cases are in a 90° rotation, which is as expected from their geometrical rotation symmetry. Such phenomenon demonstrates an excellent linearly polarized light locally at the lobes, in which the polarization distribution is as predicted in the simulation result of figure 5(c).

4. Further discussion

We made the assumption previously that the concentric-ring grating magnetic metamaterials behave as azimuthal HWPs, based on which we predict the polarization and phase manipulations from this structure with almost satisfactory experimental demonstration. However, not all features on the experiment results shown above are perfectly fitting with this

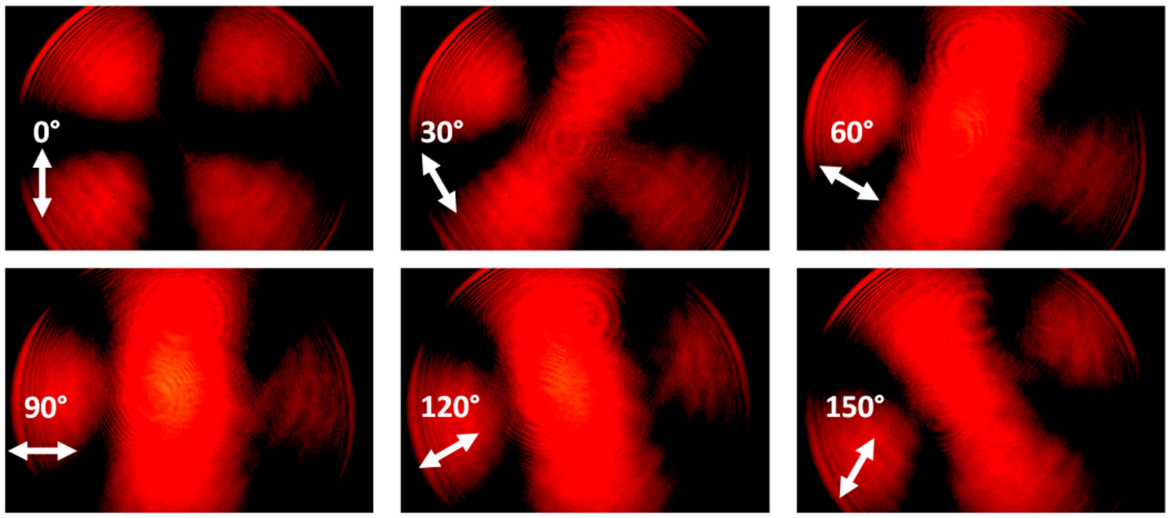

Figure 7. The measured beam transmission images after passing through a rotating polarization analyzer under incident horizontal linear polarization.

expectation. Mostly obvious from the polarization analysis shown in figures 6 and 7, it is observed that the center area of the transmitted beam, instead of being a dark spot representing the polarization singularity, is actually linearly polarized at the same direction of the incident beam. This observation indicates that the inner rings of the concentric-ring grating pattern fails to act as perfect azimuthal HWPs as the outer rings do. Indeed, the outer rings have a comparably large radius, where the fabrication errors have negligible impact; while the inner rings have small radius where the fabrication errors become significant. The fabrication errors in our samples, especially for the stitching mismatch between adjacent fabrication sections as shown in figure 4(a), has substantially affects the comprehensive light manipulation not only for polarization, but for phase, i.e. vortex generation as well. As shown in figures 4(b) and (c), not only has the generated vortex exhibited an asymmetric intensity profile, the interference pattern also exhibit the trend of vortex splitting. Instead of observing perfect double-spirals in the interference pattern, in figure 4(c) it shows a trend of two single fork-like spirals, indicating two split charge-one vortices. This phenomenon has been studied by previous literatures that the structural defect in the sample will induce higher order vortex to split into multiple fundamental charge-one vortices and make an asymmetric profile of the transmitted beam [48, 49].

This inefficiency of light manipulation induced by the structural defect can be much improved by using a more advanced fabrication tool that can read large pattern in fine resolution without the need to section the whole pattern. However, physically, the failure of equivalence between the center part of the magnetic metamaterial concentric-ring grating patterns and azimuthal HWPs is inevitable. The equivalent HWP is an 'effective medium' treatment for the macroscopic optical property of the magnetic metamaterials with at least several unitcells. For the inner rings where their curvature is large and the whole ring is subwavelength, they cannot be viewed as effective linear HWPs anymore. The center part of the concentric-ring patterns will always remain a structural defect even by a perfect fabrication.

Lastly, we discuss the potential possibilities to improve the performance of the magnetic metamaterial HWP. The magnetic metamaterials here is based on Ag–SiO_2–Ag cavity, which suffers from large losses from reflection and absorption of the metal layers. The energy efficiency will be low even if they are perfectly fabricated. To address this difficulty, except for using dense dielectrics as discussed previously, we noted that some earlier researches indicate that ferrite based magnetic material can support simultaneous magnetic and electric responsibility at low frequency regime [50, 51]. Such structures excel at both low loss due to impedance matching and thin thickness at longitudinal direction, which can be an excellent candidate to achieve HWP functionality. It is also noteworthy that some lanthanide materials exhibit magnetic dipole transition in optical frequencies, which support optical magnetism [52]. Is it possible to use the intrinsic optical magnetic materials to realize HWP functionality at sub-wavelength scale with low loss and thin thickness? This will be an interesting topic to be explored in the future work.

5. Conclusion

In summary, we have designed and demonstrated the magnetic metamaterial HWPs operating at visible wavelength with a high polarization conversion purity of 80% and a deep subwavelength thickness. The concentric-ring grating patterns of HWP elements are designed as unique integrated beam converters to produce structured light, including charge-two optical vortices under incident CP and vector beams with rotated polarization topological structures of charge two under incident LP. Our proposed magnetic metamaterial HWP structures greatly improve the polarization conversion purity of transmission-type plasmonic PBOEs, which will contribute as excellent building blocks for realizing ultra-compact metamaterial devices used in structured beam manipulation,

complex phase and polarization engineering, optical trapping, and on-chip optical communications.

Acknowledgments

The authors acknowledge support from the Office of Naval Research (N00014-16-1-2408) and the National Science Foundation (DMR-1552871, ECCS-1653032, CBET-1402743). The authors also acknowledge the facility support from the Materials Research Center at Missouri S&T. This work was performed, in part, at the Center for Integrated Nanotechnologies, an Office of Science User Facility operated for the US Department of Energy (DOE) Office of Science. Sandia National Laboratories is a multi-program laboratory managed and operated by the Sandia Corporation, a wholly owned subsidiary of the Lockheed Martin Corporation, for the US Department of Energy's National Nuclear Security Administration under contract DE-AC04-94AL85000. The author Jinwei Zeng is currently affiliated with the department of Electrical Engineering and Computer Science, University of California Irvine, Irvine, CA, 92697.

ORCID iDs

Jinwei Zeng https://orcid.org/0000-0001-5795-2406
Xiaodong Yang https://orcid.org/0000-0001-9031-3155

References

[1] Litchinitser N M 2012 Structured light meets structured matter *Science* **337** 1054–5
[2] Litchinitser N M 2016 Photonic multitasking enabled with geometric phase *Science* **352** 1177–8
[3] Molloy J E and Padgett M J 2002 Lights, action: optical tweezers *Contemp. Phys.* **43** 241–58
[4] Grier D G 2003 A revolution in optical manipulation *Nature* **424** 810–6
[5] Veysi M, Guclu C and Capolino F 2015 Vortex beams with strong longitudinally polarized magnetic field and their generation by using metasurfaces *J. Opt. Soc. Am.* B **32** 345–54
[6] Padgett M and Bowman R 2011 Tweezers with a twist *Nat. Photon.* **5** 343–8
[7] Wang J and Willner A 2014 Using orbital angular momentum modes for optical transmission *Optical Fiber Communication Conf.* (Optical Society of America) paper W4J. 5
[8] Li S and Wang J 2013 Multi-orbital-angular-momentum multi-ring fiber for high-density space-division multiplexing *IEEE Photon. J.* **5** 7101007
[9] Zhao Z, Wang J, Li S and Willner A E 2013 Metamaterials-based broadband generation of orbital angular momentum carrying vector beams *Opt. Lett.* **38** 932–4
[10] Yang X, Yao J, Rho J, Yin X and Zhang X 2012 Experimental realization of three-dimensional indefinite cavities at the nanoscale with anomalous scaling laws *Nat. Photon.* **6** 450–4
[11] Sun L, Gao J and Yang X 2013 Broadband epsilon-near-zero metamaterials with steplike metal-dielectric multilayer structures *Phys. Rev.* B **87** 165134
[12] Cai W, Chettiar U K, Yuan H–K, de Silva V C, Kildishev A V, Drachev V P and Shalaev V M 2007 Metamagnetics with rainbow colors *Opt. Express* **15** 3333–41
[13] Yuan H, Chettiar U K, Cai W, Kildishev A V, Boltasseva A, Drachev V P and Shalaev V M 2007 A negative permeability material at red light *Opt. Express* **15** 1076–83
[14] Zeng J, Wang X, Sun J, Pandey A, Cartwright A N and Litchinitser N M 2013 Manipulating complex light with metamaterials *Sci. Rep.* **3** 2826
[15] Sun J, Zeng J and Litchinitser N M 2013 Twisting light with hyperbolic metamaterials *Opt. Express* **21** 14975–81
[16] Zeng J, Gao J, Luk T S, Litchinitser N M and Yang X 2015 Structuring light by concentric-ring patterned magnetic metamaterial cavities *Nano Lett.* **15** 5363–8
[17] Richardson D, Fini J and Nelson L 2013 Space-division multiplexing in optical fibres *Nat. Photon.* **7** 354–62
[18] Niv A, Biener G, Kleiner V and Hasman E 2006 Manipulation of the Pancharatnam phase in vectorial vortices *Opt. Express* **14** 4208–20
[19] Bomzon Z, Kleiner V and Hasman E 2001 Pancharatnam–Berry phase in space-variant polarization-state manipulations with subwavelength gratings *Opt. Lett.* **26** 1424–6
[20] Chen W, Han W, Abeysinghe D C, Nelson R L and Zhan Q 2011 Generating cylindrical vector beams with subwavelength concentric metallic gratings fabricated on optical fibers *J. Opt.* **13** 015003
[21] Yu N, Genevet P, Kats M A, Aieta F, Tetienne J–P, Capasso F and Gaburro Z 2011 Light propagation with phase discontinuities: generalized laws of reflection and refraction *Science* **334** 333–7
[22] Genevet P, Yu N, Aieta F, Lin J, Kats M A, Blanchard R, Scully M O, Gaburro Z and Capasso F 2012 Ultra-thin plasmonic optical vortex plate based on phase discontinuities *Appl. Phys. Lett.* **100** 013101
[23] Arbabi A, Horie Y, Bagheri M and Faraon A 2015 Dielectric metasurfaces for complete control of phase and polarization with subwavelength spatial resolution and high transmission *Nature Nanotechnol.* **10** 937–43
[24] Sun J, Wang X, Xu T, Kudyshev Z A, Cartwright A N and Litchinitser N M 2014 Spinning light on the nanoscale *Nano Lett.* **14** 2726–9
[25] Yang Y, Wang W, Moitra P, Kravchenko I I, Briggs D P and Valentine J 2014 Dielectric meta-reflectarray for broadband linear polarization conversion and optical vortex generation *Nano Lett.* **14** 1394–9
[26] Wang W, Li Y, Guo Z, Li R, Zhang J, Zhang A and Qu S 2015 Ultra-thin optical vortex phase plate based on the metasurface and the angular momentum transformation *J. Opt.* **17** 045102
[27] Arbabi A, Horie Y, Bagheri M and Faraon A 2015 Dielectric metasurfaces for complete control of phase and polarization with subwavelength spatial resolution and high transmission *Nat. Nanotechnol.* **10** 937–43
[28] Wan W, Gao J and Yang X 2016 Full-color plasmonic metasurface holograms *ACS Nano* **10** 10671–80
[29] Zheng G, Mühlenbernd H, Kenney M, Li G, Zentgraf T and Zhang S 2015 Metasurface holograms reaching 80% efficiency *Nat. Nanotechnol.* **10** 308–12
[30] Huang L *et al* 2013 Three-dimensional optical holography using a plasmonic metasurface *Nat. Commun.* **4** 2808
[31] Ni X, Kildishev A V and Shalaev V M 2013 Metasurface holograms for visible light *Nat. Commun.* **4** 2807
[32] Berry M V 1984 Quantal phase factors accompanying adiabatic changes *Proc. R. Soc.* A **392** 45–57

[33] Berry M V 1987 The adiabatic phase and Pancharatnam's phase for polarized light *J. Mod. Opt.* **34** 1401–7
[34] Hasman E, Kleiner V, Biener G and Niv A 2003 Polarization dependent focusing lens by use of quantized Pancharatnam–Berry phase diffractive optics *Appl. Phys. Lett.* **82** 328–30
[35] Bomzon Z, Biener G, Kleiner V and Hasman E 2002 Radially and azimuthally polarized beams generated by space-variant dielectric subwavelength gratings *Opt. Lett.* **27** 285–7
[36] Karimi E, Schulz S A, De Leon I, Qassim H, Upham J and Boyd R W 2014 Generating optical orbital angular momentum at visible wavelengths using a plasmonic metasurface *Light Sci. Appl.* **3** e167
[37] Zeng J, Li L, Yang X and Gao J 2016 Generating optical orbital angular momentum at visible wavelengths using a plasmonic metasurface *Nano Lett.* **16** 3101–8
[38] Arbabi A and Faraon A 2017 Fundamental limits of ultrathin metasurfaces *Sci. Rep.* **7** 43722
[39] Yu N, Aieta F, Genevet P, Kats M A, Gaburro Z and Capasso F 2012 A broadband, background-free quarter-wave plate based on plasmonic metasurfaces *Nano Lett.* **12** 6328–33
[40] Ding F, Wang Z, He S, Shalaev V M and Kildishev A V 2015 Broadband high-efficiency half-wave plate: a supercell-based plasmonic metasurface approach *ACS Nano* **9** 4111–9
[41] Devlin R C, Khorasaninejad M, Chen W T, Oh J and Capasso F 2016 Broadband high-efficiency dielectric metasurfaces for the visible spectrum *Proc. Natl Acad. Sci.* **113** 10473–8
[42] Devlin R C, Ambrosio A, Wintz D, Oscurato S L, Zhu A Y, Khorasaninejad M, Oh J, Maddalena P and Capasso F 2017 Spin-to-orbital angular momentum conversion in dielectric metasurfaces *Opt. Express* **25** 377–93
[43] Khorasaninejad M, Chen W T, Zhu A Y, Oh J, Devlin R C, Rousso D and Capasso F 2016 Multispectral chiral imaging with a metalens *Nano Lett.* **16** 4595–600
[44] Backlund M P, Arbabi A, Petrov P N, Arbabi E, Saurabh S, Faraon A and Moerner W E 2016 Removing orientation-induced localization biases in single-molecule microscopy using a broadband metasurface mask *Nat. Photon.* **10** 459–62
[45] Schulz S A, Upham J, Bouchard F, De Leon I, Karimi E and Boyd R W 2015 Quantifying the impact of proximity error correction on plasmonic metasurfaces *Opt. Mater. Express* **5** 2798–803
[46] Wang D *et al* 2015 Switchable ultrathin quarter-wave plate in terahertz using active phase-change metasurface *Sci. Rep.* **5** 15020
[47] Wang D, Gu Y, Gong Y, Qiu C and Hong M 2015 An ultrathin terahertz quarter-wave plate using planar babinet-inverted metasurface *Opt. Express* **23** 11114–22
[48] Ricci F, Löffler W and van Exter M 2012 Instability of higher-order optical vortices analyzed with a multi-pinhole interferometer *Opt. Express* **20** 22961–75
[49] Maleev I D and Swartzlander G A 2003 Composite optical vortices *J. Opt. Soc. Am.* B **20** 1169–76
[50] Liu S, Chen W, Du J, Lin Z, Chui S T and Chan C T 2008 Manipulating negative-refractive behavior with a magnetic field *Phys. Rev. Lett.* **101** 157407
[51] Chen H, Lu W, Li J, Yu J, Lin Z, Chan C T and Liu S 2017 Manipulating unidirectional edge states via magnetic plasmonic gradient metasurfaces *Plasmonics* **12** 1079–90
[52] Kasperczyk M, Person S, Ananias D, Carlos. L D and Novotny L 2015 Excitation of magnetic dipole transitions at optical frequencies *Phys. Rev. Lett.* **114** 163903